PERGAMON

International Journal of Multiphase Flow 26 (2000) 245–265

International Journal of Multiphase Flow

www.elsevier.com/locate/ijmulflow

Pressure gradient and particle adhesion in the pneumatic transport of cohesive fine powders

F.-J. Wang, J.-X. Zhu*, J.M. Beeckmans

Department of Chemical and Biochemical Engineering, The University of Western Ontario, London, Ontario, Canada, N6A 5B9

Received 23 March 1998; received in revised form 13 January 1999

Abstract

Pneumatic transport of Group C 20 μm glass beads was studied in a 31.7 mm vertical line, along with 66 μm Group A glass beads for comparison. Pressure gradients along the riser were measured and the Zenz type state diagrams were constructed for both type of particle. For Group C particles, the results show that the Zenz diagram has the usual characteristic form, but the minimum pressure gradient is much lower and is positioned at a significantly higher gas velocity. Multiple layers of Group C particles were found to adhere to the column wall, while only a fraction of the column inner surface was covered by the 66 μm particles. The effects of the electrostatics effect during solids conveying was also examined through the addition of anti-static particles and was shown to be less significant for the finer particles. This is because the tube inner surface is entirely covered by the particulates, which reduces the charging since only like materials are then in contact.

Keywords: Ultrafine powder; Cohesive powders; Pneumatic transport; Particle adhesion; Electrostatics

1. Introduction

1.1. Pressure gradient and Zenz diagram

Fine particles, especially Group C particles, have been considered as cohesive and very difficult to transport due to their strong interparticle forces (Marcus et al., 1990), and only

* Corresponding author. Tel.: +1-519-661-2131; fax: +1-519-661-3498.
E-mail address: jzhu@julian.uwo.ca (J.X. Zhu).

0301-9322/00/$ - see front matter
PII: S0301-9322(99)00009-9

limited information on the conveying of such materials is available in the literature (Boothroyd, 1966; 1967; 1971; Yang et al., 1980; Rastogi and Klinzing, 1992). However, these particles, with high surface-to-volume area, are advantageous in many chemical and physical processes. On the other hand, fine powders are generally harmful to health and polluting to the environment when handled manually. Pneumatic transport, a contained solids handling method, may significantly reduce or even eliminate those disadvantages. For these reasons it was deemed important to investigate the applicability of pneumatic transport of such particles.

Predicting the pressure drop is often a key factor in designing a pneumatic transport system to meet both technical and economical requirements. However, when examining the existing literature, there are almost no theoretical or experimental studies applicable to Group C particles. All of the correlations applicable to conveying of coarse particles seem to suffer a large degree of departure from the experimental data when applied to fine particle systems. This is because that in the fine particle transport system a number of additional factors come into play. For example, it is almost impossible to know the effective particle size in the process as particle agglomeration is bound to occur with such particles (especially Group C particles). Furthermore, the fine particles tend to adhere to the wall and form a layer covering the pipe. This is expected to significantly affect the solids friction factor by altering the shear force exerted on solids flow by the pipe wall, which, in turn, greatly changes the overall pressure gradient. These factors all serve to complicate the modeling of fine particles systems.

Little work has been done so far to address this problem. One of the rare attempts to predict the pressure gradient for fine particles systems was made by Yousfi and Gau (1974a, 1974b), who obtained a constant solids friction factor of 0.00015 for 20 μm glass beads over a limited range. Yang et al. (1980) proposed a new equation to calculate the solids friction factor for fine particles by assuming that the gas–solid slip velocity in the conveying line equals the terminal velocity of solid particles. They claimed that the following equation was successfully applied to fine nuclear fuel powders with average particles size between 1 and 2 μm:

$$f_p = 0.0126\frac{(1-\varepsilon)^{0.021}}{\varepsilon^3} \tag{1}$$

where ε is the voidage and f_p is the solids friction factor ($f_p = 4f_s$) which is solids friction factor defined in Eq. (6).

Boothroyd (1966; 1967) did a series of studies on gaseous suspension flow of fine particles with size ranging up to 40 μm and reported the pressure drop and turbulence characteristics. He correlated the friction pressure gradient data with several dimensionless parameters, W_s/W_g, $\rho_g D^2/\rho_p d_p^2$ and Re_D, which were based on gaseous fluid mechanics theory (where W_g is the gas mass flow rate, W_s is the solids mass flow rate, d_p is the mean particle diameter, Re_D is the Reynolds number related to pipe diameter $= U_g D\rho_g/\mu$, and U_g is the superficial air velocity). His results suggested that whereas the variation of pressure drop in tubes containing a suspension of large particles is usually linear with solids loading, this become less clear with fine particles. It should be noticed that the above three studies were only for dilute phase transport under very specific experimental conditions. No proof was shown that they can be extended to cover general operation conditions within the entire dilute phase regime, because

very little experimental data are available on the fine particle transport. No correlation is available in the literature to predict pressure gradient in transport of fine particles.

The Zenz diagram (Zenz and Othmer, 1960) has been widely adopted to describe the flow behavior in various operations employing pneumatic transport. Since there are currently no reliable and generalized theoretical models available to characterize the transport of Group C particles, constructing the widely used Zenz type phase diagram would be of importance in characterizing the flow conditions in fine particle transport systems and to serve as the initial design criterion. The only reported work was carried out by Rastogi and Klinzing (1992), who tested the possibility of pneumatic transport of 20 μm coal particles and found that the Zenz type diagrams was valid for this Group C powder.

1.2. Effects of electrostatic charges

The effect of electrostatic charge is often important in powder handling process, particularly in pneumatic conveying. However, results reported on this phenomenon have always been paradoxical. This situation may be described by Klinzing's famous remark (Klinzing, 1981): "Often, if an explanation cannot be found for an observation, electrostatics is named as the cause. Or, if someone wants to complicate a discussion of gas–solid flow, the issue of electrostatics is interjected".

During powder handling operations, particles make frequent contact with the surface of the wall and invariably become electrically charged due to the process of contact electrification. When two dissimilar materials make and then break contact, charge transfer from one material to the other occurs, a process known as tribo-electrification (Bailey, 1984). The materials of the pipe, ranging from conductor to insulator, play a crucial role in the charge transfer process. The electrostatic charge may in some circumstances alter the dynamics of the pneumatic transport process. There are reports that electrostatic charges may cause a significant increase of pressure drop in the transport line (Richardson and Mcleman, 1960; Yousfi and Gau, 1974a, 1974b), although this phenomenon is not observed in all gas–solid systems (Muzyka, 1985; Sen Gupta, 1994). So far, the literature on quantitative measurement of pressure drop along transport lines in the presence of electrostatic charging is scarce.

Normally, a larger electrostatic charge per particle is expected with smaller particles (Klinzing, 1981; Marcus et al., 1990). However, in his particle adhesion study Bowling (1986) considered the electrostatic factor as predominant only for particles with diameter greater than 50 μm, and Boothroyd (1966) reported that little electrostatic effect was observed when transporting fine particles (Group C particles). They suggested that with the suspensions of very fine particles, the entire inside surface of the pipe may have been coated with a layer of the solids so that the column wall has identical surface properties to the flowing particles and therefore charge transfer is attenuated.

1.3. Particle adhesion in pneumatic transport lines

During powder handling operations, particles, especially if fine, may adhere strongly to the surface. Numerous studies in the literature have only focused on particle adhesion to surfaces under static conditions. Among the few publications on fine particle conveying, no attention

was paid to particle adhesion on the tube. When particles flow through a pipe, a fraction of them will deposit on the wall surface. The quantity of the deposition on the wall is mostly meager for large particles, but the tendency for very fine particles to stick to the wall becomes large (Klinzing, 1981). Eventually, a layer of particles will cover the whole surface of the wall. After a layer has formed on the wall, the particles in the suspension will interact with this layer of particles instead of with the tube material directly, altering the frictional and electrostatic behavior of the flow. Usually, the force of adhesion for fine particles, particularly Group C particles, is large enough to hold particles on the wall with great tenacity. Increasing the transport gas velocity may blow away some of the adhered particles, however, it is impossible to clean up all the particles on the wall by the hydrodynamic shear force exerted by the fluid.

Despite the importance of particle adhesion in fine particle conveying, there is so far only a sparse general understanding of particle adhesion phenomena. The difficulty may be attributed to the complexity of the adhesion forces, as those forces are usually a combination of physical and chemical forces, in addition to mechanical stress. The present study was carried out to answer some of the important questions raised above and to achieve a general understanding of the pneumatic transportation and wall adhesion of fine Group C powders, under different operating conditions, with or without the effect of electrostatics.

2. Experimental details

2.1. Apparatus

A schematic of the vertical pneumatic transport unit is shown in Fig. 1. It consisted of a 31.7 mm i.d. plexiglass tube with a height of approximately 10 m, a fluidized bed solids feeder, two cyclones, a bag filter and another similar plexiglass tube used as the solids return line. The fluidized bed feeder also acted as a solids inventory, and was 0.25 m in diameter and 1.25 m in height. Solids were introduced from the fluidized bed feeder into the transport line through an orifice in its submerged section. The solids feeding rate was finely controlled by adjusting the pressure difference between the fluidized bed and the transport line. Before the particles reached the cyclones, the suspension flowed through a stabilizing zone and then through the test section. Pressure taps were mounted axially along the transport line to measure the pressure gradient, using water manometers. After being separated from the gas–solids suspension by the cyclones, particles flowed back into the feeder via the returning line. An acrylic diverter valve was installed in the return line to allow the measurement of the solids flow rate. The gas stream with unrecovered particles from the cyclones was sent to the bag filter for final clean-up and after joining with air vented from solids feeder, went to the lab exhaust system.

Air entering the system was split into two streams. One stream was introduced to the fluidized bed feeder, the other was used as transport air. The flow rates of fluidizing air and transport air were measured with a rotameter and an orifice plate flow meter respectively. In addition to the manual valve control, solenoid valves were installed upstream of each manually operated valve to provide instantaneous shut down of the air supply to the system. The relative

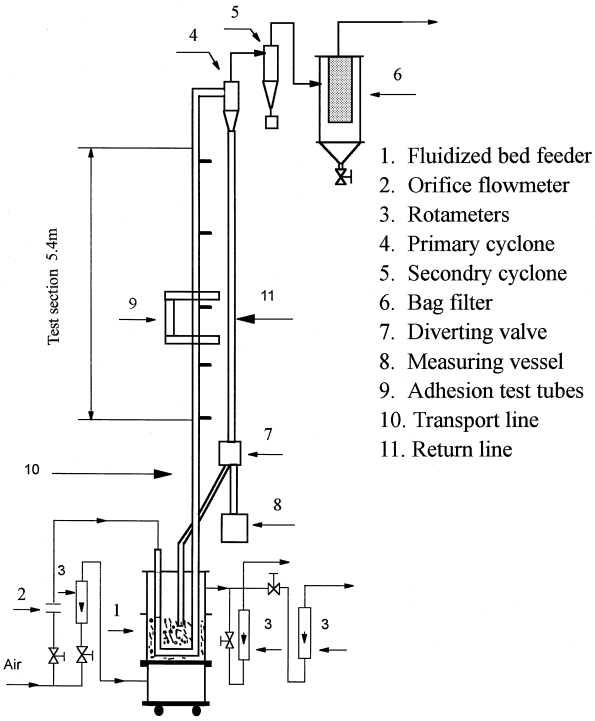

Fig. 1. Schematic view of experimental installation.

humidity of the air was measured with wet-and-dry bulb thermometers placed upstream of the orifice plate meter in the transport air line. At the present experimental conditions, the relative humidity was between 25% and 35% to prevent the marked increase of particle cohesiveness.

During the current study, particle adhesion in the pneumatic transport line was investigated using so-called 'adhesion test tubes'. As shown in Fig. 2, the adhesion test tubes consisted of two parts, the slide carriages and the 'twin tube'. The slide carriage was made of two 234 × 94 × 16 mm plexiglas plates, each with a 6.35 mm deep rectangular slot. The width of this slot was exactly the same as the outside diameter of the tube in the transport line. A hole of the same inside diameter (31.7 mm) as the transport tube was opened on the center of both plates. Four 3.1 mm holes were drilled around the center holes so that the plates could be connected to the flanges of the transport line. This arrangement allowed an accurate fit between the holes on the plates and the tube of the transport line. On the other end of the slide carriage, another 31.7 mm i.d. hole was drilled on the bottom plate with a small piece of plexiglas tube glued beneath it, were used to withdraw the collected particles. A distance of 79.3 mm was kept between the centers of the side and the centre holes. The 'twin-tube' was in fact two 0.35 m long 31.7 mm i.d. plexiglas tubes held together 79.3 mm apart from each other's centers. The tubes were identical with the transport line and were used to ensure good alignment and fitting between the test tubes and the transport line. A 6.35 mm thick sponge called 'wraptite' was glued on the tubes to ensure a good seal and smooth movement of the twin-tube. During a run the twin-tube was in its rightmost position as viewed in Fig. 2. Adhering particles could be

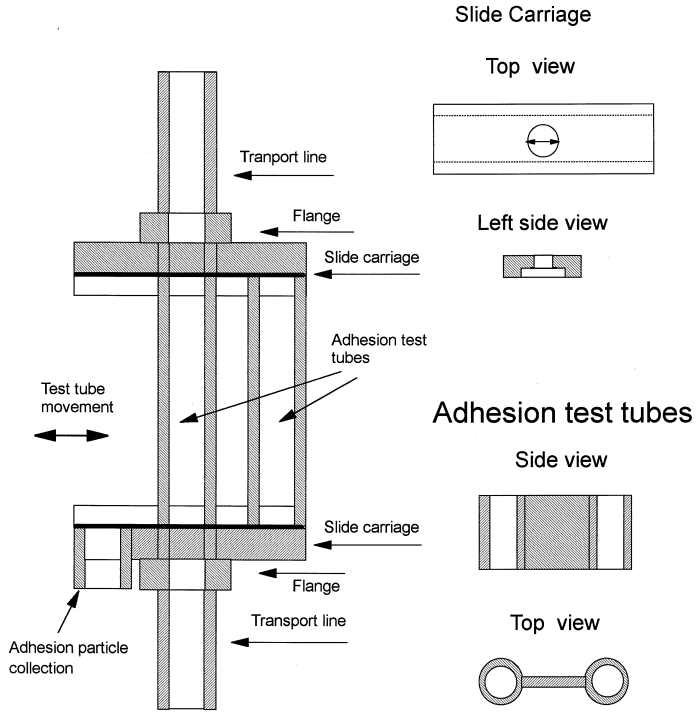

Fig. 2. Schematic view of adhesion test tubes.

collected at any time with minimal disturbance to the flow by moving the twin-tube rapidly to the left. After adhering particles had been collected the twin-tube was returned to its normal position on the right.

2.2. Operating procedure

Before each experiment, the two valves to control air vented from the fluidized feeder were turned to wide open to avoid any pressure buildup. The adhesion test tube was positioned in accurate alignment with the transport line. At the start up stage of the experiments, the valve to transport air was initially opened up to the desired level. After the transport air had flowed for a while, the fluidizing air was turned on. The fluidizing air velocity was kept at a multiple of 1.5 to 3 times the minimum fluidization velocity of the particles. Different solids flow rates were achieved by adjusting the bed pressure. Tuning of the fine control valve for the air vent from the fluidized bed was used to control fluctuations in the solids feed rate. When the solids return rate equaled the solids feed rate, the level of solids inventory in the feeder became constant and steady state was considered established. The system would be then kept running for about 10 to 20 min before the measurements were made.

When the data acquisition was finished, the solenoid valves were activated to shut down the air virtually instantaneously. The valve for venting the fluidized bed air was turned completely open to release the pressure in the bed. Particle adhesion data were taken next. The adhesion

tube was gently slid into the particle collecting position. A pre-weighed plastic bag was next placed underneath the withdrawal tube. First, the tube was tapped evenly with a small rubber hammer to shake off the adhering particles until no more fell off. Then the adhesion tubes were taken off, and the rest of the particles were brushed off. Particles collected by the above methods were weighed separately and referred to as 'tapped particles' and 'brushed particles', respectively. The samples of both types of adhesion particles were analyzed with a Brinkman particle size analyzer to obtain their size distributions. Before changing from the 20 μm glass beads to the 66 μm glass beads, anti-electrostatic particles (Larostat 519®) were added to the system at 0.5% by weight of the inventory and additional runs were made to investigate the effect of electrostatics on the pressure gradient. Similar runs with Larostat were made with the 66 μm beads.

2.3. Properties of particles

Two types of glass beads from Potters (Montreal, Quebec) were used in the present research. The smaller glass beads had a mean area–volume diameter of 20 μm, and are located in the Group C region close to the C–A boundary in Geldart's diagram (Geldart, 1973). The other type was a typical Group A powder with a mean diameter of 66 μm. Both particles are of spherical shape. The density of both sizes of particles was 2500 kg/m^{2}s and their minimum fluidization velocities were measured in the fluidized bed feeder. The 66 μm glass beads had a U_{mf} of 5.5 mm/s and showed the typical Group A fluidization characteristics. On the other hand, with a U_{mf} of 0.4 mm/s, the 20 μm particle system possessed more complex characteristics typical of Group C particles. The particle size distribution for the 20 μm particles are shown in Fig. 10. The 66 μm particles also have a normal size distribution. The particle size distributions were also regularly monitored with the Brinkman particle size analyzer. Size analyses performed at various times during the course of the study showed that the average particle size did not change much and that the losses from the primary cyclone and attrition of the particles were minimal.

The anti-electrostatic powder added to the system is available commercially under the name 'Larostat® 519' and has been reported to successfully diminish the electrostatic charge (Ham, 1992; Salah, 1995). It is a white ammonia-based compound (40% silica and 60% quaternary ammonia) with an average particle size of 20 μm.

3. Results and discussions

3.1. Visual observation

In the 20 μm glass bead system, once the solids were introduced into the transport line, particles were immediately seen to deposit on the pipe wall. At low solids flux and high air velocity the gas–solids flow patterns could be observed through the partially covered plexiglas tube. When the air velocity was reduced, more and more particles accumulated on the tube wall. Layers of particles covering the entire inside surface of the pipe began to

appear, making visual observation almost impossible. Although it is usually expected that smaller particles generate greater electrostatic charge (Klinzing, 1981), characteristic electrostatic phenomena such as the noise of discharging and electric sparks were barely observed throughout the experiments with 20 μm glass beads. These observations differed from expectation for fine particles based on the reports in the literature, although similar observations had been reported by Boothroyd (1966). He reported that only minor electrostatic charging occurred during the transport of zinc particles in the size range of 0–40 μm.

By contrast, little particle deposition was seen on the pipe wall during the transport of 66 μm glass beads, and visual observation for this system was much easier than for the 20 μm glass beads system. When the solids flux was low and the solids velocity was high, particles were seen being lifted by the air stream in a uniformly dispersed suspension, and clusters (referring to all types of particle aggregations, as defined in the broad sense by Bi et al. (1993)) were seldom observed. However, clusters began to appear as the air velocity was reduced. Further decreasing the air velocity caused higher solids concentrations near the wall than in the center of the pipe. Eventually, internal solids recirculation was seen in the wall region. Also, a lot of electrostatic charging was observed throughout the experiments, especially when the air velocity was raised above 8 m/s. The sound of discharging was very loud and sparks could be seen along the transport tube notwithstanding the grounding. After 0.5% by weight of Larostat was added into the system, the intensity of electrostatics charging was not seen to be significantly reduced.

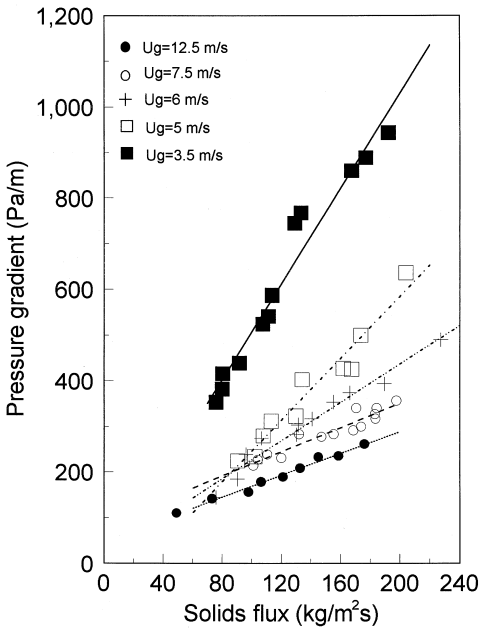

Fig. 3. Pressure gradient as a function of solids flux for the 20 mm glass beads system.

3.2. Pressure gradient and solids friction factor

The pressure gradients along the transport line with 20 μm glass beads are presented in Fig. 3 (U_g is the superficial gas velocity). All the pressure gradient data plotted in the figures were collected from the fully developed region in the transport line. (The fully developed region was considered to be reached when the derivative of the pressure gradient becomes zero.) It can be seen that at constant solids flux the pressure gradient increases with decreasing air velocity. This suggests that the pressure gradient is more sensitive to solids flux at low air velocity and more sensitive to the air velocity at high solids flux.

Voidage data were not collected in this study. However, since the diameter of the particles employed in this study was about 20 μm, it seems reasonable to assume that the slip velocity equals the terminal velocity of the particles when the air velocity is high (2). The solids concentration can then be inferred directly from the solids circulation rate (3). It should be noted that the above assumption is not true at low air velocity, as solids may flow in the conveying line in the forms of clusters which greatly increase the effective particle size. This assumption is only made for the purpose of investigating if the existing correlations can be directly applied to Group C particles.

Based on this assumption, one can then also calculate the friction factor and the solids concentration:

$$V_p = V_g - V_t \tag{2}$$

$$(1-\varepsilon) = \frac{G_s}{(\rho_p V_p)} \tag{3}$$

where V_g and V_p are the actual gas and particle velocities. V_t is the single particle terminal velocity, $(1-\varepsilon)$ is the solids concentration. G_s is the solids circulation rate and ρ_p is the particle density. Since the overall pressure drop in the fully developed region in the vertical pneumatic transport can be broken down to its individual contributions, one can express it as follows:

$$\Delta P = \Delta P_{static} + \Delta P_{friction} \tag{4}$$

The static contribution due to the particles can be expressed as:

$$\Delta P_{static} = \rho_p(1-\varepsilon)\Delta L g \tag{5}$$

Here ΔP is pressure drop across the given tube section, ΔP_{static} is the pressure drop due to static head from the gas-particle suspension, $\Delta P_{friction}$ is the pressure drop due to friction loss, ε is the bed voidage and ΔL is the length of the given tube section.

The frictional contribution can also be divided into two parts, the gas-wall frictional loss and the solids-wall frictional loss. The pressure drop due to gas-wall friction loss, ΔP_{fg}, is frequently assumed to be equivalent to that due to gas alone and is given as follows:

$$\Delta P_{fg} = \frac{2 f_g \rho_g \varepsilon V_g^2 \Delta L}{D} \tag{6}$$

where ΔP_{fg} is the pressure drop due to gas friction loss, ρ_g is the gas density, D is pipe inner diameter and $f_g = 0.079/Re^{0.25}$ is Fanning gas friction factor.

The pressure drop due to solids-wall frictional loss, ΔP_{fs}, is usually defined as:

$$\Delta P_{fs} = \frac{2 f_s \rho_p (1-\varepsilon) V_p^2 \Delta L}{D} \tag{7}$$

where ΔP_{fs} is the pressure drop due to solids friction loss, and f_s is the solids friction factor.

Unlike the case of the gas friction factor, there is not a generalized equation to obtain solids friction factors. In this study, three of the most representative equations, proposed by Konno and Saito (1969), Capes and Nakamura (1973) and Yang (1978) (Eqs. (8–10) respectively) were used to obtain the solids friction factor for 20 μm glass beads at a particle velocity of 12.5 m/s.

$$f_s = \frac{0.0285}{V_p (gD)^{0.5}} \tag{8}$$

$$f_s = \frac{0.048}{V_p^{1.22}} \tag{9}$$

$$f_s = \frac{0.0126(1-\varepsilon)^{0.021}}{\varepsilon^3} \tag{10}$$

where D is the tube diameter. The solids friction factor can be calculated from experimental data as follows:

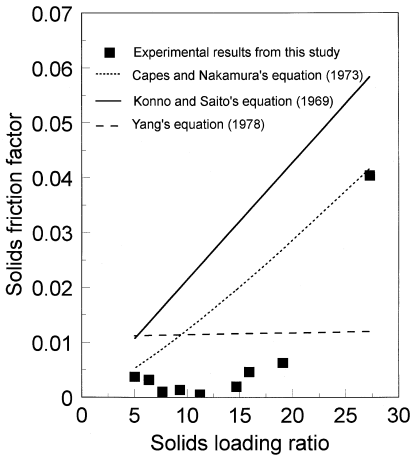

Fig. 4. Comparison of experimentally obtained and preicted solid friction factors.

$$f_s = \frac{\Delta P/\Delta L - \rho_p(1-\varepsilon)\cdot g - 2f_g\rho_g\varepsilon V_g/D}{2\rho_p(1-\varepsilon)V_p/D} \tag{11}$$

The solids friction factors calculated from Eqs. (8–10) are compared with those obtained experimentally using Eq. (11) (see Fig. 4). It is clearly shown that the experimentally obtained solids friction factors are much smaller than the predictions of the three equations. This indicates that the Group C particles have unique properties and that the existing equations developed from coarse particles are not valid for such particles. The decreased values may result from the fact that with the entire inner surface covered with fine particles, the friction loss is caused by the interactions between the suspension and the layer of deposited particles on the pipe material. When the particles are being conveyed, some particles in the suspension will deposit on the pipe wall and others will be picked up by the gas. This process keeps the particles in the adhesion layer refreshed and this may have a lubricating action which reduces friction. From the above comparison, it can be concluded that Group C particles have significantly different flow characteristics due to their strong interparticle force.

3.3. Zenz diagrams

Zenz diagrams were constructed using pressure gradient data (Fig. 5). The straight line represents the pressure gradients of gas flowing alone in the transport line, while the other three curves correspond to the solids fluxes of 175, 140 and 90 kg/m^{2}s respectively. It can be

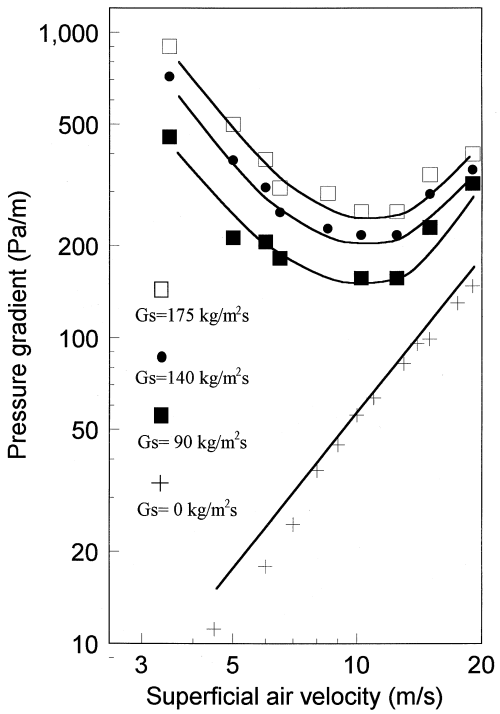

Fig. 5. Zenz plot for the 20 mm glass beads system.

seen from the figure that the curves for 20 μm glass beads exhibit the typical characteristics of the Zenz diagram. As the superficial air velocity is reduced from 19 to 3.5 m/s at constant solids flux, the gradients for 20 μm glass beads all experience the same behavior in which they drop initially, reach the minimum, and then rise again. For 20 μm glass beads, the 'minimum pressure gradient point' is located approximately at 11 m/s.

The Zenz diagram for 66 μm glass beads is plotted together with data obtained with the 20 μm particles in Fig. 6, at solids flux of 86 and 177 kg/m^{2}s. Like the 20 μm glass beads, the pressure gradient curves for 66 μm glass beads also display the features of a typical Zenz plot. The pressure gradient minimum point was determined to be at a velocity of 6.5 m/s.

However, some disparities in flow characteristics also exist between 66 and 20 μm glass beads systems. The minimum pressure gradients for 20 μm glass beads are smaller than those for 66 μm glass beads at the same solids flux. This is understandable, since the voidage is much larger for the finer particles given their lower slip velocity. In addition, the 66 μm glass beads system experienced the pressure minimum at a much lower air velocity than the 20 μm glass beads system. It is a common practice to have dilute pneumatic transport systems operate at a velocity slightly higher than the one corresponding to the pressure minimum in order to conserve energy. The result that the 20 μm glass bead system reaches the pressure minimum at a much higher air velocity is contrary to the common assumption that a higher gas velocity is required for the transport of larger and denser particles. However, this general rule is determined from the commonly employed materials, which do not include Group C particles. The phenomenon of a higher minimum pressure gradient velocity for fine particles has not been reported previously. It is, therefore, useful to discuss the mechanism that causes this

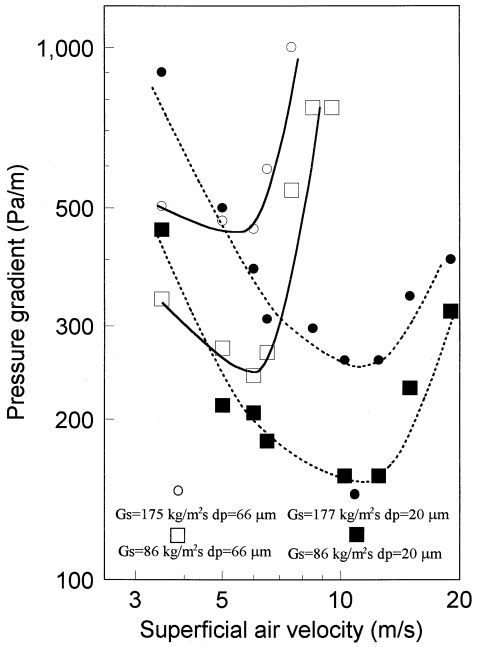

Fig. 6. Comparison of the Zenz plots for the 20 and 66 mm glass beads systems.

phenomenon. Essentially, the shift of the minimum pressure gradient point to the right is due to a reduction of suspension-to-wall friction. For 20 μm fine particles, the friction due to the solids-wall interaction is likely to be much smaller than that for the 66 μm glass beads, due to the reduced particle size. Secondly, as conjectured above, the deposit-pickup process of the adhered particles may act as lubrication and cause a further reduction in solids friction. On the Zenz plot, the frictional loss is the dominant contributor to the total pressure gradient on the right-hand side of the pressure minimum, and the solids head loss makes up the majority of the total pressure gradient on the left-hand side of the pressure gradient minimum. As the air velocity is reduced from a high value, the frictional loss decreases and the solids head loss increases. At the pressure gradient minimum point, the contribution of the solids head loss to the total pressure drop begins to exceed that of the friction loss. Since it was found out that the frictional loss of Group C particles is smaller, it is not surprising that solids head contribution surpasses the frictional contribution with such particles and that the system reaches the minimum pressure gradient point at much higher air velocity.

It is interesting to note that the 20 μm particle system behaved much differently from the system using 66 μm glass beads, although they were both conventionally considered fine particles in the pneumatic transport field. The significant discrepancy in flow characteristics between Group A and Group C particles clearly indicates that the existing design criteria developed for large particles should not be applied in the design of systems with very fine particles. Thus, the availability of Zenz diagrams for Group C particles is of importance for the design of a fine particle pneumatic transport system.

3.4. Electrostatic charging

During the present experiments, differences in the magnitude of the electrostatic charging were observed for the two gas–solids flow systems. In some of the experimental studies, Larostat 519® was added into the transport system at a concentration of 0.5% by weight to reduce the electrostatics. At this concentration, the presence of Larostat was shown to not have a significant effect on the flow characteristics of the glass bead particles (Salah, 1995).

The pressure gradients of both particle systems in the presence of Larostat are illustrated in Fig. 7 as functions of the solids flux. From the figure, it can be seen that the addition of Larostat did lower the pressure gradients for both the 20 μm glass beads and the 66 μm glass beads systems. The relative effect, however, was much larger for the 66 μm particles. Compared with the 20 μm particles, the pressure gradients with 66 μm glass beads were significantly reduced over the current experimental range after the Larostat particles were introduced into the system. This indicates that electrostatics plays an important role in the conveying of the larger particles, but a minimal role for the Group C particles. For the 66 μm particles, this anti-electrostatic additive also appears to have a much larger effect in reducing the pressure, the higher the velocity, consistent with the results of Masuda et al. (1976).

In general, the electrostatic charging which occurred in the present experiments increased the pressure gradients along the transport line for both gas–solids systems, and its influence on the pressure gradients became stronger with increasing air velocity and increasing particle size. According to Klinzing (1981), the smaller the diameter of the flowing particles, the greater the electrostatic charge generated. The reverse results were found in the present study. Both visual

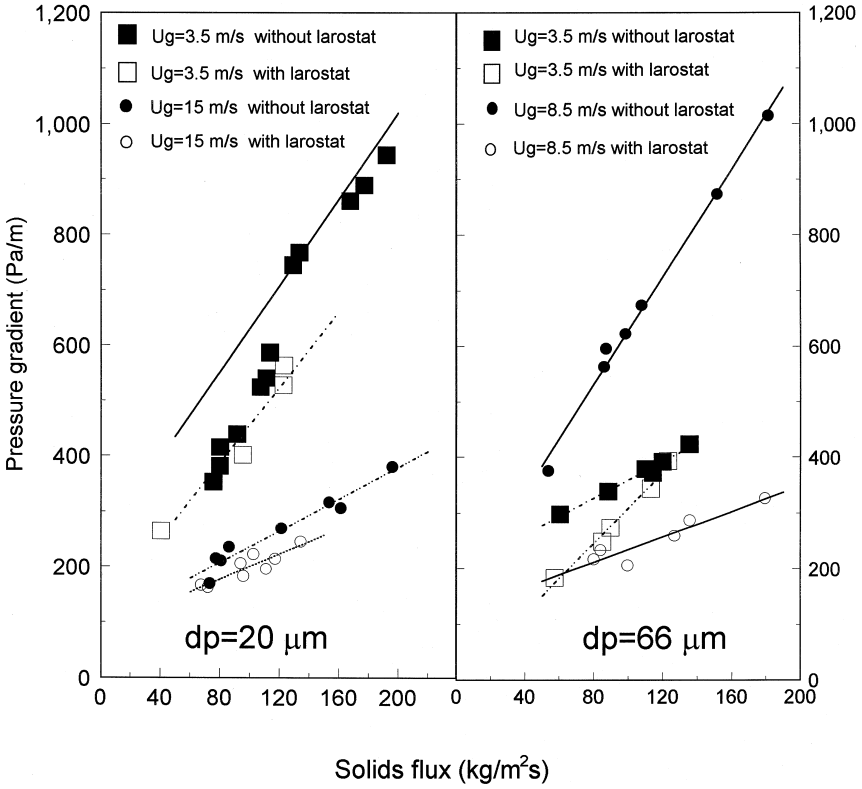

Fig. 7. Effect of Larostat on the pressure gradiant of the 20 and 66 mm glass beads systems.

observation and pressure gradient data indicate that the 20 μm glass beads generate much smaller electrostatic charging than the 66 μm glass beads. The reason is that because the surface of the tube is completely covered with adhering particles (see next section) no charging by tribo-electrification can occur.

The electrostatic charging also affects the structure of the Zenz diagram. Fig. 8 shows that the pressure gradients of 20 μm glass beads at solids flux of 100 kg/m^{2}s was slightly lowered after the Larostat particles were introduced into the system. The pressure gradient minimum in the presence of Larostat is basically located at the same velocity as before. From the figure, it can also be seen that the addition of Larostat particles only had a small effect on the Zenz diagram for Group C particles. This suggests that electrostatics charging is not an important factor in the pneumatic transport of 20 μm glass beads.

In contrast, the presence of Larostat powder made a significant impact on the Zens plot of 66 μm glass beads system, as shown in Fig. 8. As the air velocity decreases, the pressure gradient for conditions with Larostat drops slowly towards the minimum point instead of the quick fall in the conditions observed without Larostat. The transition from dilute phase transport to dense phase transport was changed from sharp to smooth after the anti-electrostatic particles were added. Apparently, strong electrostatic charging occurs in the larger

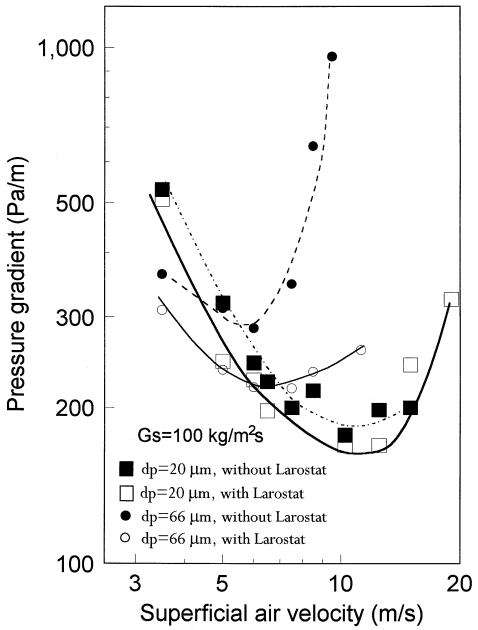

Fig. 8. Effect of Larostat on the Zenz plots for the 20 and 66 mm glass beads systems.

particle systems without the anti-electrostatic agent and this causes significant changes to the characteristics of the flow.

3.5. Particle adhesion

During powder handling and conveying operations, particles, especially fine particles, may adhere strongly to the tube surface. It is believed that particle adhesion may have a powerful effect on the characteristics of gas–solids suspension flow in a pipe. This is because after the initial deposition of fine particles on the pipe wall, the particles in suspension will interact with those adhering to the wall, causing frictional and electrostatic behaviors which differ from those anticipated from interactions between particles and the pipe wall materials alone. This, however, has not received much attention, although particle adhesion may be important in pneumatic transport.

In the current experimental studies, particle adhesion measurements were carried out with the 'adhesion test tubes' shown in Fig. 2 and with the procedure described earlier to collect the adhered particles. Each set of particle adhesion data was divided into two groups: the 'tapped' particles which were collected while gently tapping the test tube and the 'brushed' particles which were obtained by brushing off the remaining particles from the test tube. It should be noted that this classification is somewhat arbitrary but nonetheless helps reveal the nature of the adhesion condition on the wall. Since no information on particle adhesion in gas–solid transport system is available in the literature, a parameter called 'equivalent layer thickness' is introduced to quantify the particle adhesion on the transport tube. The 'equivalent layer

Table 1
Equivalent particle adhesion layer thickness (mm) for 20 μm glass beads

Air velocity (m/s)	Collection method	Particle rate (±5) (kg/m^{2}s)			
		65	85	105	130
3.5	Tapping	0.3555	0.2811	0.3802	0.3149
	Brushing	0.0039	0.0027	0.0142	0.0255
8.5	Tapping	0.1739	0.1515	0.2114	0.1748
	Brushing	0.0093	0.0128	0.0119	0.0107
10.3	Tapping	0.0432	0.0544	0.0539	0.0583
	Brushing	0.0071	0.0079	0.0059	0.0056
19.0	Tappping	0.0070	0.0183	0.0279	0.0251
	Brushing	0.0020	0.0028	0.0045	0.0042

thickness', h, is defined as follows:

$$h = m/\pi D l \rho_b \tag{12}$$

where m is the mass of particles collected, D is the inside diameter of the tube, and l is the length of the tube and ρ_b particle bulk density.

As stated above, the pneumatic transport system using 20 μm glass beads exhibits much different flow behavior from the conveying system with 66 μm glass beads, and the strong particle adhesion is considered a major cause of those differences. It is therefore critical to understand particle adhesion. All experiments were conducted without the addition of the anti-static Larostat particles.

Results of the studies conducted to investigate the effect of solids flux on particle adhesion of 20 μm and 66 μm glass beads are presented in Tables 1 and 2. From Table 1, one can find that for 20 μm particles the particle layer formed by the 'tapped' particles generally does not vary much with increasing solids fluxes at air velocities of 3.5, 8.5 and 10.3 m/s. However, at the air

Table 2
Equivalent particle adhesion layer thickness (mm) for 66 μm glass beads

Air velocity (m/s)	Collection method	Particle rate (±5) (kg/m^{2}s)			
		65	85	105	130
3.5	Tapping	5.27	6.24	7.47	6.02
	Brushing	0.78	0.80	1.08	0.98
6.0	Tapping	12.06	n/a	22.20	30.49
	Brushing	1.30	n/a	0.74	1.21
7.5	Tapping	21.47	n/a	19.16	29.88
	Brushing	1.57	n/a	1.46	1.76
9.5	Tapping	27.71	41.52	43.09	56.64
	Brushing	1.06	6.25	2.83	6.20

velocity of 19 m/s, the 'tapped' adhesion layer initially increases when the solids flux is raised from 65 to 105 kg/m^{2}s, and then levels off with further increase in solids flux. On the other hand, the 'brushed' particle adhesion layer fluctuates within a limited range at 8.5 and 10.3 m/s in spite of the change of solids flux, and increases with solids flux at air velocities of 3.5 and 19.0 m/s.

The mechanism by which particle adhesion is affected by the air velocity is not fully understood. It is probable that a saturated adhesion layer exists at each air velocity. At the saturation condition, the adhesion forces (van der Waals and electrostatic), reach an equilibrium with the drag force exerted by the air. Thus, in a stable gas–solid flow system, particle adhesion will eventually achieve the saturation point if particles can fully interact with pipe. Once the adhesion equilibrium is established, the thickness of the adhered particle layer will no longer change with the length of operation.

The results of adhesion studies with 66 μm glass beads are shown in Table 2. Compared with 20 μm glass beads, much fewer 66 μm glass beads deposited on the wall. The adhesion of 66 μm glass beads exhibits a different trend from that of 20 μm glass beads. The thickness of the 'tapped' particle adhesion layer increases slowly with solids flux, while the results with the 'brushed' adhesion layer looks very scattered over the range of solids fluxes studied, possibly because of the limited amount of particles collected in this manner for the 66 μm glass beads (less than 0.1 g). The trend of increasing adhesion with solids flux becomes more significant when the operating air velocity is raised to 9.5 m/s. At this velocity, the 'tapped' adhesion layer thickness increases from about 0.027 mm at 65 kg/m^{2}s to about 0.056 mm at 130 kg/m^{2}s.

The reason that particle adhesion increases with solids flux may be attributed to the electrostatic phenomenon prevailing in the experiments with 66 μm beads. It is known that the primary forces which act to bring particles to a surface and then hold them there are van der Waals forces and electrostatic forces (Bowling, 1986). Electrostatic forces predominate for particles larger than 50 μm, while van der Waals forces predominate for particles with smaller diameter. Thus, it can be inferred that the electrostatic force is the major force contributing to the adhesion of 66 μm glass beads. In dry pneumatic transport systems, there is clear evidence that the electrostatic charge increases with solids loading and air velocity for Group A particles, as shown by the results presented early in this work and by previous studies (Klinzing, 1981; Masuda et al., 1976). Therefore, as the solids flux is increased, the adhesion forces rise with the increasing electrostatic forces.

One would tend to imagine that the lower the air velocity, the thicker the adhesion layer covering the tube, because air at lower velocity causes a much smaller hydrodynamic drag force on the adhered particles. However, the current experimental results of particle adhesion for both beads at various air velocities show a different picture. The equivalent layer thickness for both particle systems at $G_s = 125$ kg/m^{2}s is presented as a function of operating air velocity in Fig. 9. For 20 μm glass beads, both 'tapped' layers and 'brushed' layers do grow thicker as the air velocity is reduced for $U_g > 6.0$ m/s; i.e., more particles adhere to the pipe wall with reduced air velocity, just as anticipated. However, the quantity of particle adhesion begins to drop as the air velocity is further reduced from 6.0 to 3.5 m/s. This phenomenon seems to contradict common sense but it may be related to the increased solids reflux near the wall. As some solids begin to recirculate downwards in the wall region, they may exert a downward drag force on the particles deposited on the wall and peel off some adhered particles.

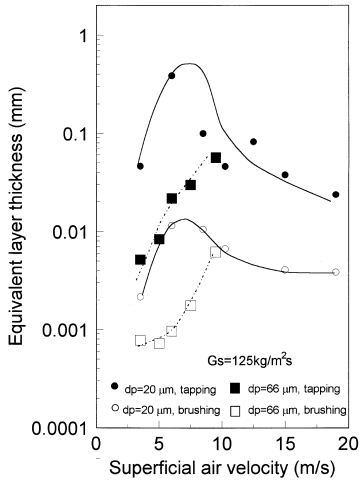

Fig. 9. Particle adhesion of 20 and 66 mm glass beads.

In contrast to the 20 μm glass beads system, the particle adhesion layer for 66 μm glass beads grows in thickness with increasing transport air velocities. This reverse trend may be caused by a different adhesion mechanisms for the two types of particles. According to Bowling (1986), electrostatic force is the dominant adhesion force for 66 μm glass beads, while the van der Waals force is the primary adhesion force for 20 μm glass beads. As was pointed out previously, in a dry pneumatic transport system the electrostatic forces increase with solid flux and air velocity. Therefore, as the air velocity is increased, the growth in total adhesion force may exceed the increase of drag force exerted by air for 66 μm glass beads, resulting in more particles adhering to the wall. On the other hand, the van der Waals forces are mainly related to the particle properties and are generally not affected by the air velocity. As a result, the total adhesion forces remain basically at the same value for 20 μm glass beads, regardless the air velocity. In addition, the complete coverage of the column inner surface by the 20 μm particles also discourages the generation of electrostatics and an increase of velocity has been shown earlier not to change this fact. Thus, increasing air velocity would lead to a decrease in particles adhesion from the finer particles as a result of increased drag forces on the particles.

Fig. 9 shows that the adhesion of 20 μm glass beads is very strong in the present pneumatic transport system. At 6.0 m/s, the particles deposited on the wall form the thickest adhesion layer, which is equivalent to 20 times the particle size. Even at a velocity of 19.0 m/s, the highest air velocity investigated, the total adhesion layer thickness is still about 0.04 mm, twice the particle diameter. The above results indicate that the adhesion of 20 μm glass beads creates multiple particle layers covering the entire inner surface of the tube. Thus, instead of contacting the pipe, the gas–solid suspension actually interacts with the particle layer covering the wall surface. With particles covering the surface of the wall, the solid-wall friction will be altered. Therefore, particle adhesion should be seriously considered and taken into account in designing a pneumatic transport system for very fine particles. On the other hand, Fig. 9 shows that the highest adhesion layer thickness is only 45 μm for the 66 μm beads, less than one diameter, and therefore the inner pipe wall surface is only partially covered. It can be

concluded that when the 66 μm glass beads are conveyed in the transport line, the gas–solids suspension will interact with a rough pipe surface resulting from the only partially covered column wall. Hence, a higher roughness factor than that for a smooth tube should be employed in estimating the wall friction loss.

According to the definitions of the two types of collected adhesion particles, 'tapped' particles are collected before 'brushed' particles. In other word, 'tapped' particles are located at the outer layer of the adhered particles, while 'brushed' particles attached closer to the wall. Throughout the adhesion experiments it was found that the 'tapped' particles make up the majority of the particles adhering to the wall. During the experiments conducted with 20 μm glass beads, the collected particles were analyzed with a Brinkman particle size analyzer. The results are shown in Fig. 10, and the average particle diameter of the 'tapped' particles is found to be 18.7 μm, almost the same as that of the flowing particles in the transport line. On the other hand, the mean particle diameter of the 'brushed' particles was only 11.7 μm, significantly smaller than that of the 'tapped' particles. This suggests that among particles adhered to the pipe wall, the particles first adhering to the column wall are smaller then the mean size, while other adhering particles have comparable size with the particles in suspension. It may also be assumed that the 'tapped' particles exchange with the particles in the suspension flow throughout the duration of the solids transport, while the 'brushed' particles remain more or less stagnant at the inner layer of the adhered particles. To understand this distribution in the adhered particles, one needs to examine the process of particle adhesion. In general, particle movement from suspension to surface is controlled by three basic steps (Reed, 1986): particles arriving at a surface, particles bouncing back or sticking upon impact, and particles being re-suspended. Compared with larger particles, the smaller sized particles have relatively greater adhesion force and less momentum to rebound, and therefore have a better chance of

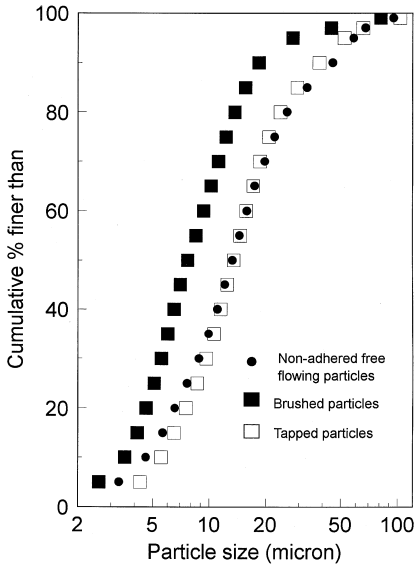

Fig. 10. Particle size distribution of adhered particles ($G_s = 127$ kg/m^{2}s, $U_g = 3.5$ m/s).

sticking to the surface and not being re-suspended again. As a result, the inner layer of adhered particles will be mainly occupied by smaller particles.

4. Conclusion

1. Pneumatic transport of 20 μm glass beads was found to be feasible in the current equipment setup.
2. The Zenz diagram for Group C powders has the normal form. It can be used to characterize flow behavior in the pneumatic conveying of Group C particles and to serve as the initial design criterion.
3. Compared with 66 μm glass beads, with the 20 μm beads the minimum pressure gradient is lower and minimum pressure gradient point is located at much higher air velocity in the Zenz plot.
4. Electrostatic charging during the transportation of 20 μm glass beads is much less significant than for 66 μm glass beads.
5. Particle adhesion for the 20 μm glass beads is very significant, with multiple layers of adhered particles collecting at the column inner wall surface, while this phenomenon was not observed with the 66 μm glass beads.
6. Among the particles adhered to the wall, the smaller particles adhered closest to wall surface, while larger particles located farther from the wall.

Acknowledgements

The authors are grateful to Wylton Enterprises, Vancouver, and the Natural Sciences and Engineering Research Council of Canada (NSERC) for their financial supports of this study. The first author would also like to thank the University of Western Ontario to provide the facilities and supports for his graduate research project.

References

Bailey, A.G., 1984. Electrostatic phenomena during powder handling. Powder Technol 37, 71–85.

Bi, H-T., Zhu, J-X., Jin, Y., Yu, Z-Q., 1993. Forms of particle aggregations in CFB. In: Proc. 6th National Conf. on Fluidization. October 3–6, Wuhan, China, 162–167.

Boothroyd, R.G., 1966. Pressure drop in duct flow of gaseous suspensions of fine particles. Trans. Instn. Chem. Engrs 44, T306–T343.

Boothroyd, R.G., 1967. Turbulence characteristics of the gaseous phase in duct flow of a suspension of fine particles. Trans. Instn. Chem. Engrs 45, T297–T310.

Boothroyd, R.G., 1971. Flowing Gas–Solids Suspensions. Chapman and Hall, London, England.

Bowling, R.A., 1986. A theoretical review of particle adhesion. In: Mittal, K.L. (Ed.), Particles on Surfaces 1: Detection, Adhesion, and Removal. Proceedings of a Symposium Held in Conjunction with Seventeenth Annual Meeting of the Fine Particles Society, July 28–August 2, San Francisco, CA. Plenum Press, New York, pp. 129–142.

Capes, C.E., Nakamura, K., 1973. Vertical pneumatic conveying—an experimental study with particles in the intermediate and turbulent flow regimes. Can. J. Chem. Eng 51, 31–38.

Geldart, D., 1973. Types of gas fluidization. Powder Technol 7, 285–292.

Ham, R.W. 1992. Effects on humidity and electrostatics on fluidized bed characteristics of cracking catalyst, Ph.D. Dissertation, The University of Western Ontario, London, Canada.

Konno, H., Saito, S., 1969. Pneumatic conveying of solids through straight pipes. J. Chem. Eng. Japan 2, 211–219.

Klinzing, G.E., 1981. Gas–Solid Transport. McGraw-Hill, New York.

Marcus, R.D., Leung, L.S., Klinzing, G.E., Rizk, F., 1990. Pneumatic Conveying of Solids. Chapman and Hall, New York.

Masuda, H., Komatsu, T., Linoya, K., 1976. The static electrification of particles in gas–solid pipe flow. AIChE J 22, 558–564.

Muzyka, D.W. 1985. The use of probabilistic multiphase flow equations in the study of the hydrodynamics and heat transfer in gas–solids suspensions. Ph.D. Dissertation, The University of Western Ontario, London, Canada.

Rastogi, S., Klinzing, G.E., 1992. Pneumatic transport of dry ultrafine coal and analysis of pressure signals. Particulate Sci. Technol 10, 21–32.

Reed, J., 1986. The adhesion of small particles to a surface. In: Mittal, K.L. (Ed.), Particles on Surfaces 2: Detection, Adhesion, and Removal. Proceedings of a Symposium Held in Conjunction with Seventeenth Annual Meeting of the Fine Particles Society, July 28–August 2, San Francisco, CA. Plenum Press, New York, pp. 3–18.

Richardson, J.F., Mcleman, M., 1960. Pneumatic conveying. Trans. Ins. Chem. Engrs 38, 257–266.

Sen Gupta, S.K. 1994. Effects of line inclination on the hydrodynamics of riser transort in the non-slugging dense phase flow regime. Ph.D. Dissertation, University of Western Ontario, London, Canada.

Salah, M., 1995. Hydrodynamics of circulating fluidized bed with internals. Master Thesis, The University of Western Ontario, London, Ontario, Canada.

Yang, W.C., 1978. A correlation for solid friction factor in vertical pneumatic conveying lines. AIChE J 24, 548–551.

Yang, W.C., Eckhardt, D.A., Skriba, M.C., 1980. Dilute phase pneumatic transport of fine nuclear fuel powders. In: Pneumotransport 5, Proc. 5th Int. Conf. on the Pneumatic Transport of Solids in Pipes, April 16–18, 309–324.

Yousfi, Y., Gau, G., 1974a. Aérodynamique de l'Ecoulement Vertical de Suspensions Concentreés Gaz–Solides—I. Regimes d'Ecoulement et Stabilité Aérodynamique. Chem. Eng. Sci. 29, 1939–1946.

Yousfi, Y., Gau, G., 1974b. Aérodynamique de l'Ecoulement Vertical de Suspensions Concentreés Gas–Solides—II. Chute de Pression et Vitesse Relative Gaz–Solide. Chem. Eng. Sci. 29, 1947–1953.

Zenz, F.A., Othmer, D.F., 1960. Fluidization and Fluid-Particle Systems. Reinhold, New York.